Original Article

The differential diagnosis of lung precursor glandular lesions, micro-invasive adenocarcinoma, and invasive adenocarcinoma using low dose spectral computed tomography perfusion imaging

Mai-Lin Chen[#], Yu-Liang Liu[#], Hai-Bin Zhu[#], Xiao-Ting Li, Li-Ping Qi, Ying-Shi Sun

Key Laboratory of Carcinogenesis and Translational Research (Ministry of Education/Beijing), Department of Radiology, Peking University Cancer Hospital & Institute, Beijing, China

Contributions: (I) Conception and design: YS Sun, ML Chen, YL Liu, HB Zhu; (II) Administrative support: YS Sun, ML Chen, YL Liu, HB Zhu; (III) Provision of study materials or patients: ML Chen, YL Liu, HB Zhu; (IV) Collection and assembly of data: ML Chen, YL Liu, HB Zhu, LP Qi; (V) Data analysis and interpretation: ML Chen, YL Liu, HB Zhu, XT Li; (VI) Manuscript writing: All authors; (VII) Final approval of manuscript: All authors.

[#]These authors contributed equally to this work.

Correspondence to: Ying-Shi Sun, MD. Key Laboratory of Carcinogenesis and Translational Research (Ministry of Education/Beijing), Department of Radiology, Peking University Cancer Hospital & Institute, 52 Fucheng Road, Haidian District, Beijing 100142, China. Email: sys27@163.com.

Background: Few studies about the association between computed tomography (CT) perfusion imaging parameters and invasiveness in lung adenocarcinoma (LUAD) have been conducted using low dose spectral CT perfusion imaging. The purpose of this study was to investigate application of spectral revolution CT low-dose perfusion imaging in the differential diagnosis of different pathological subtypes of LUAD.

Methods: This was a cross-sectional study based on historical data from January 2018 to May 2019 in Peking University Cancer Hospital & Institute. A total of 62 cases were enrolled, including 2 cases of atypical adenomatous hyperplasia (AAH), 3 cases of adenocarcinoma in situ (AIS), 4 cases of minimally invasive adenocarcinoma (MIA), and 53 cases of invasive adenocarcinoma (IAC), all confirmed with pathology. The inclusion and exclusion criteria were regulated. Using Revolution low-dose CT perfusion imaging (GE, USA), the CT perfusion parameters of hemodynamics were obtained: blood flow (BF), blood volume (BV), impulse residue function time of arrival (IRF TO), maximum slope of increase (MSI), mean transit time (MTT), permeability surface area product (PS), positive enhancement integral (PEI), and maximum enhancement time (Tmax). Univariate analysis of variance (ANOVA) or Kruskal-Wallis test was used to compare the differences of CT perfusion quantitative parameters among AAH, AIS, MIA, and IAC. Mann-Whitney test was used to compare the difference of CT perfusion imaging parameters between preinvasive lesions (AAH and AIS) and invasive lung cancer (MIA and IAC).

Results: Statistically significant differences in IRF TO were observed in LUAD with different invasiveness, namely, among AIS, MIA, and IAC groups (0.56±0.74 *vs.* 0.54±1.08 *vs.* 4.39±2.19, P=0.004). Statistically significant differences in IRF TO were also observed between pre-invasive lesions group (AAH and AIS) and invasive lung cancer group (MIA and IAC) (1.12±1.27 *vs.* 3.75±2.79, P=0.031), and between AAH + AIS + MIA groups and IAC group (0.83±1.13 *vs.* 4.12±2.69, P<0.001). There were no statistically significant differences in other CT perfusion parameters of hemodynamics among different pathological subtypes of LUAD (P>0.05).

Conclusions: The low-dose perfusion parameter IRF TO of revolution CT has the potential to be employed in the differential diagnosis of different pathological subtypes of LUAD.

Keywords: Spectral; computed tomography (CT); lung adenocarcinoma (LUAD); perfusion; quantitative analysis

Submitted Apr 12, 2023. Accepted for publication Nov 10, 2023. Published online Jan 02, 2024.
doi: 10.21037/qims-23-487
View this article at: https://dx.doi.org/10.21037/qims-23-487

Introduction

Lung cancer is the most prevalent malignant tumor with the highest morbidity and mortality rates in adults worldwide (1-3). Lung adenocarcinoma (LUAD) is the most common histological type of lung cancer, which is divided into precursor glandular lesions, minimally invasive adenocarcinoma (MIA), and invasive adenocarcinoma (IAC), according to the 2011 International Association for the Study of Lung Cancer (IASLC), American Thoracic Society (ATS) and European Respiratory Society (ERS), and 2021 World Health Organization (WHO) new classification of LUAD (4,5). Precursor glandular lesions are further divided into atypical adenomatous hyperplasia (AAH) and adenocarcinoma in situ (AIS). The invasiveness, clinical treatment, and prognosis differ among different pathological types. The overall survival rate has been reported at almost 100% for both precursor glandular lesions and MIA with complete resection; however, the prognosis of IAC is poor, with a 5-year survival rate of 49–84% (6,7). Traditional chest computed tomography (CT) can be used to evaluate the invasiveness of LUAD or the prognosis based on the morphology of the lesion edge (such as burr, lobulation), ground-glass density ratio, solid component size, and so on (8). The hemodynamic alterations of pulmonary lesions can be evaluated with non-invasive functional CT perfusion imaging techniques (9,10). The perfusion parameters include blood flow (BF), blood volume (BV), impulse residue function time of arrival (IRF TO), maximum slope of increase (MSI), mean transit time (MTT), permeability surface area product (PS), positive enhancement integral (PEI), time to peak (TTP), and maximum enhancement time (Tmax). To evaluate the hemodynamic characteristics of pulmonary nodules objectively, a new CT mode was established through quantitative multi-parameter analysis, which provides an alternative to evaluate invasive LUAD (4). Previous studies have mainly focused on the differentiation of benign and malignant pulmonary nodules, the differentiation of different pathological types of lung cancer, and the efficacy evaluation of LUAD. There is no available study on the relationship between CT perfusion parameters and different subtypes of LUAD (11-13).

The purpose of this study was to investigate the value of low dose CT perfusion imaging parameters (BF, BV, IRF TO, MSI, MTT, PS, PEI, TTP, and Tmax) to differential diagnosis of different pathological subtypes of LUAD. We present this article in accordance with the STROBE reporting checklist (available at https://qims.amegroups.com/article/view/10.21037/qims-23-487/rc).

Methods

Subjects

The study was conducted in accordance with the Declaration of Helsinki (as revised in 2013). The study was approved by the Medical Ethics Committee of Peking University Cancer Hospital & Institute (No. 2021KT04), and written informed consent was provided by all patients.

This was a cross-sectional study based on historical data. In this study, a total of 62 cases were enrolled in Peking University Cancer Hospital & Institute from January 2018 to May 2019. The inclusion criteria were as follows: (I) aged over 18 years, males or female; (II) diameter of the lesion greater than 6 mm; and (III) the diagnosis was confirmed with surgical pathology and biopsy. The exclusion criteria were as follows: (I) history of contrast agent allergy; (II) severe liver and renal insufficiency, thyroid toxicity; and (III) pregnant and lactating women. The detailed inclusion and exclusion criteria for patient selection are shown in *Figure 1*.

Preparation before examination

Before spectral CT perfusion scanning, the cases were informed of the specific examination process, precautions, and potential complications. After removing all foreign bodies that may interfere the chest scan, a blue indwelling needle was placed in the right anterior elbow vein of the patient. The chest and abdomen were fixed with a belt, and the subject was instructed to breathe calmly to reduce

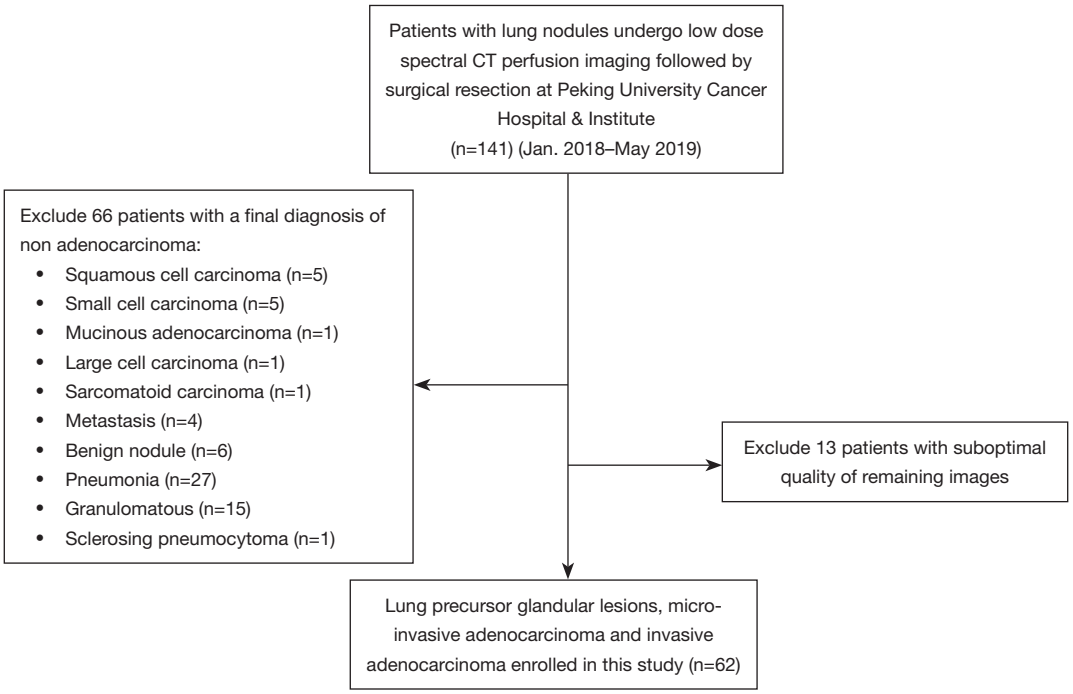

Figure 1 Detailed inclusion and exclusion criteria for patient selection. CT, computed tomography.

respiratory motion artifacts on the image.

Scan technique

Revolution Xtream CT (GE Healthcare, Waukesha, WI, USA) was used. Cases were scanned from the apex of the lung to the diaphragm at the bottom of the lung in direction from head to foot. A routine chest scan was performed first before CT perfusion imaging scanning was taken. The technical parameters of the CT scans were as follows: tube voltage 120 kVp, automatic milliampere technology, pitch 0.984, noise index 9.00, rotation time of X-ray tube ball 0.6 s per circle, scan field of view (SFOV) =500 mm, collimator width 40 mm, layer thickness 5 mm, and matrix 512×512. The group injection method was used in the right elbow median vein. At 5 seconds after injection of contrast medium, a continuous dynamic scanning of the local target lesion was performed, with a range of 16 mm and a duration of 40 seconds, and the dynamic perfusion basic image was obtained. Non-ionic iodine contrast agent iohexol Injection (300 mgI/mL) was used as contrast agent, and the injection flow rate and injection dosage were determined based on previous studies (12,14), with adjustment for the Chinese population. For cases with a body weight equal to or less than 70 kg, a dosage of 40 mL and an injection rate of 5 mL/s were used; for cases with a body weight more than 70 kg, a dosage of 50 mL and an injection rate of 6 mL/s were used. This was followed by a 30 mL physiological saline injection at the same rate, which is conducive to reflecting the blood perfusion state of lesions.

Image post-processing

The original basic image of dynamic perfusion imaging was transmitted to GE AW4.7 workstation for image post-processing. Perfusion images of pulmonary nodules were analyzed by two senior radiologists with Perfusion 4 analysis software (GE Healthcare). The aorta or main branch at the same level was selected as the feeding artery, and the region of interest (ROI) of pulmonary nodules and aorta were drawn respectively. The ROI was placed on the maximum cross section of the lesion, with an area of 1/3–2/3 of the lesion, avoiding liquefaction, necrosis, bleeding, calcification, and pulmonary vessels and bronchus. All tumors were assessed twice with an interval of 1 week, and the average value was calculated. The following CT perfusion imaging parameters of pulmonary nodule were obtained: BF, BV, IRF TO, MSI, MTT, PS, PEI, TTP, and Tmax.

Table 1 Basic information of the 62 patients with lung adenocarcinoma with different invasiveness

Clinical features	Number
Age (median, years)	60
Sex, n (%)	
Female	36 (58.1)
Male	26 (41.9)
Smoking, n (%)	
Yes	20 (32.3)
No	42 (67.7)
Density, n (%)	
Pure GGN	5 (8.1)
Mixed GGN	34 (54.8)
Solid	23 (37.1)
Pathological classification, n (%)	
AAH	2 (3.2)
AIS	3 (4.8)
MIA	4 (6.5)
IAC	53 (85.5)

GGN, ground-glass nodule; AAH, atypical adenomatous hyperplasia; AIS, adenocarcinoma in situ; MIA, micro-invasive adenocarcinoma; IAC, invasive adenocarcinoma.

Pathology evaluation

Biopsied lesion specimens were fixed with 10% neutral formalin, routinely embedded in paraffin, continuously sliced with 4 μm thickness, and stained with hematoxylin and eosin (HE). After HE staining, two senior pathologists (Wei Sun, MD and Xin Yang, MD, both with 12 years of experience in pathological diagnosis of lung cancer) confirmed the diagnosis without any information regarding the patients. The histological morphology was evaluated according to the 2011 IASLC/ATS/ERS LUAD standard and the 2021 WHO histological classification of lung tumors, and a comprehensive histological classification was performed. The lesions with diameter ≤3 cm and tumor cells growing on alveolar wall without interstitial, vascular, and pleural infiltration were defined as AIS. The lesions with diameter ≤3 cm, tumor cells adherent to the alveolar wall, interstitial infiltration range ≤5 mm, and no vascular and pleural infiltration were defined as MIA. The range of interstitial infiltration >5 mm was classified as IAC (5). Concurrently, immunohistochemical envision two-step method was used to detect antibodies P40, TTF-1, Napsin A, and Ki67.

Statistical analysis

The measurement data were expressed as mean ± standard deviation. Intraclass correlation coefficients (ICCs) were used to assess the reliability of perfusion parameters. ICCs less than 0.5, between 0.5 and 0.75, between 0.75 and 0.9, and greater than 0.90 are indicative of poor, moderate, good, and excellent reliability, respectively (15). Parameters with ICC ≥0.75 were included for further analysis. The quantitative parameters BF, BV, IRF TO, MSI, MTT, PS, PEI, TTP, and Tmax of spectral CT perfusion imaging of LUAD nodules in three groups (AIS, MIA, IAC) were compared by one-way analysis of variance (ANOVA) or Kruskal-Wallis test. Comparison was made between groups using Bonferroni method. The P value was corrected by Bonferroni method for multiple comparisons between groups. Mann-Whitney test was used to compare the parameters of CT perfusion imaging between the two groups of LUAD: precursor glandular lesions (AAH and AIS) and invasive lung cancer (MIA and IAC). All P values were two-sided. A P value <0.05 was considered statistically significant. All data analyses were performed using the software SPSS 18.0 (IBM Corp., Chicago, IL, USA).

Results

Clinical results

Thus, a total of 62 patients including 26 men and 36 women [median age 60 years, interquartile range (IQR) 42–81 years] were enrolled, including 23 cases of solid density and 39 cases of ground-glass density (*Table 1*). Pathological results showed AAH in 2 cases (3.2%), AIS in 3 cases (4.8%), MIA in 4 cases (6.5%), and IAC in 53 cases (85.5%). All lung cancers were confirmed by biopsy or surgical pathology.

Comparison of quantitative parameters of AIS, MIA, and IAC of lung cancer in spectral CT perfusion imaging

All the perfusion parameters were highly reliable (ICCs ≥0.75). The comparison results of spectral CT perfusion imaging parameters of AIS, MIA, and IAC are shown in *Tables 2-4* and *Figures 2-4*. For the quantitative parameters of spectral CT perfusion imaging among AIS, MIA, and

Table 2 Comparison of CT perfusion parameters among AIS, MIA, and IAC

Parameters	AAH (n=2)	AIS (n=3)	MIA (n=4)	IAC (n=53)	P value
BF (mL/min/100 g)	11.92	91.63±80.16	74.55±90.06	55.27±42.42	0.703
BV (min/100 g)	0.15	2.98±2.64	2.38±2.88	2.49±2.18	0.629
IRF TO (s)	2.79	0.56±0.74	0.54±1.08	4.39±2.19	0.004
MSI (%)	6.63	6.23±2.13	17.98±14.81	12.98±7.95	0.440
MTT (s)	–	2.41±0.22	2.63±0.90	5.43±3.46	0.437
PS (mL/min/100 g)	1.05	14.92±5.01	16.86±19.64	14.13±18.45	0.563
PEI (HU)	25.95	0.07±0.08	0.10±0.13	0.34±0.43	0.642
Tmax (s)	0.12	1.83±1.88	3.68±6.37	6.26±3.28	0.225
TTP (s)	9.54	12.77±11.36	17.35±9.96	17.75±7.96	0.905

The data are presented by mean ± SD. CT, computed tomography; AIS, adenocarcinoma in situ; MIA, micro-invasive adenocarcinoma; IAC, invasive adenocarcinoma; AAH, atypical adenomatous hyperplasia; BF, blood flow; BV, blood volume; IRF TO, impulse residue function time of arrival; MSI, maximum slope of increase; MTT, mean transit time; PS, permeability surface area product; PEI, positive enhancement integral; HU, Hounsfield units; Tmax, maximum enhancement time; TTP, time to peak; SD, standard deviation.

Table 3 Comparison of CT perfusion parameters between AAH + AISs and MIA + IACs

Parameters	MIA + IACs (n=57)	AAH + AISs (n=5)	P value
BF (mL/min/100 g)	62.94±63.15	71.71±76.63	0.985
BV (min/100 g)	2.68±2.53	2.27±2.58	0.699
IRF TO (s)	3.75±2.79	1.12±1.27	0.031
MSI (%)	11.83±8.99	6.33±1.75	0.183
MTT (s)	4.16±3.07	1.95±0.80	0.201
PS (mL/min/100 g)	13.25±16.16	10.24±12.60	0.602
PEI (HU)	0.36±0.96	0.09±0.07	0.900
Tmax (s)	5.16±4.06	4.40±4.64	0.787
TTP (s)	17.64±10.41	13.63±9.66	0.826

The data are presented by mean ± SD. CT, computed tomography; AAH, atypical adenomatous hyperplasia; AIS, adenocarcinoma in situ; MIA, micro-invasive adenocarcinoma; IAC, invasive adenocarcinoma; BF, blood flow; BV, blood volume; IRF TO, impulse residue function time of arrival; MSI, maximum slope of increase; MTT, mean transit time; PS, permeability surface area product; PEI, positive enhancement integral; HU, Hounsfield units; Tmax, maximum enhancement time; TTP, time to peak; SD, standard deviation.

IAC, there were significant differences in IRF TO value among the three groups (0.56±0.74 *vs.* 0.54±1.08 *vs.* 4.39±2.19 s, P=0.004). It was gradually increased in AISs or MIAs, compared with IACs (*Table 2*, *Figures 2-4*). There was no missing data for each variable of interest.

In the precursor glandular lesions (AAH + AIS) and lung invasive carcinomas (MIA + IAC) cohort, 5 precursor glandular lesions and 57 lung invasive carcinomas were assessed. Raw variables for differentiating AAH + AISs from MIA + IACs are shown in *Table 3*.

The quantitative parameters of IRF TO between AAH + AISs and MIA + IACs were (1.12±1.27 *vs.* 3.75±2.79 s, P=0.031), IRF TO of AAH + AISs was faster than that of MIA + IACs.

In the 100% disease-specific survival (DSS) lesions (AAH + AIS + MIAs) and IACs cohort, 9 DSS 100% lesions and 53 IACs were assessed (*Table 4*). These raw variables for differentiating AAH + AIS + MIAs from IACs are shown in *Table 4*. The IRF TO value of group AAH + AIS + MIAs was also significantly shorter than that of IACs (0.83±1.13

Table 4 Comparison of CT perfusion parameters between AAH + AIS + MIAs and IACs

Parameters	IACs (n=53)	AIS + AAH + MIAs (n=9)	P value
BF (mL/min/100 g)	61.75±61.25	73.13±77.42	0.813
BV (min/100 g)	2.71±2.53	2.33±2.53	0.461
IRF TO (s)	4.12±2.69	0.83±1.13	<0.001
MSI (%)	11.22±8.23	12.11±1155	0.857
MTT (s)	4.24±3.12	2.23±0.81	0.138
PS (mL/min/100 g)	12.89±16.03	13.55±15.68	0.860
PEI (HU)	0.38±1.00	0.09±0.10	0.968
Tmax (s)	5.27±3.93	4.04±5.00	0.361
TTP (s)	17.67±10.96	15.49±9.30	0.374

The data are presented by mean ± SD. CT, computed tomography; AAH, atypical adenomatous hyperplasia; AIS, adenocarcinoma in situ; MIA, micro-invasive adenocarcinoma; IAC, invasive adenocarcinoma; BF, blood flow; BV, blood volume; IRF TO, impulse residue function time of arrival; MSI, maximum slope of increase; MTT, mean transit time; PS, permeability surface area product; PEI, positive enhancement integral; HU, Hounsfield units; Tmax, maximum enhancement time; TTP, time to peak; SD, standard deviation.

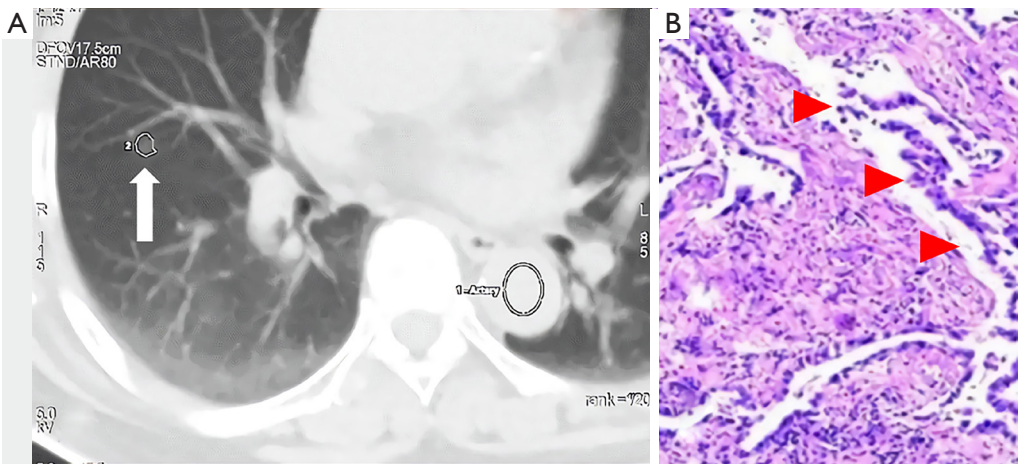

Figure 2 A 67-year-old female with right middle lobe AIS was examined by spectral CT perfusion imaging. (A) The CT image of the patient. (B) The pathology image of the patient. (A) Axial CT image at the lung window showed a pure ground-glass opacity in the right middle lobe (arrow). (B) The diagnosis of AIS (red arrowheads) was confirmed by pathology (H&E staining at ×400 magnification). CT perfusion parameter IRF TO was 1.43 s, which was correlated with the pathological diagnosis of AIS. AIS, adenocarcinoma in situ; CT, computed tomography; H&E, hematoxylin and eosin; IRF TO, impulse residue function time of arrival.

vs. 4.12±2.69 s, P<0.001).

There was no significant difference in BF, BV, MSI, MTT, PS, PEI, TTP, and Tmax among different types of LUAD (P>0.05).

Discussion

According to the 2011 IASLC/ATS/ERS classification of LUAD, the prognosis of LUAD is mainly affected by its pathological invasiveness. At present, it is difficult to obtain the preoperative pathological diagnosis of ground-glass nodules. High-resolution chest CT is often used to estimate the invasiveness of ground-glass nodules, and corresponding treatment measures are formulated. Previous traditional chest CT studies have suggested that the density of nodules, solid components, CT value, ground-glass

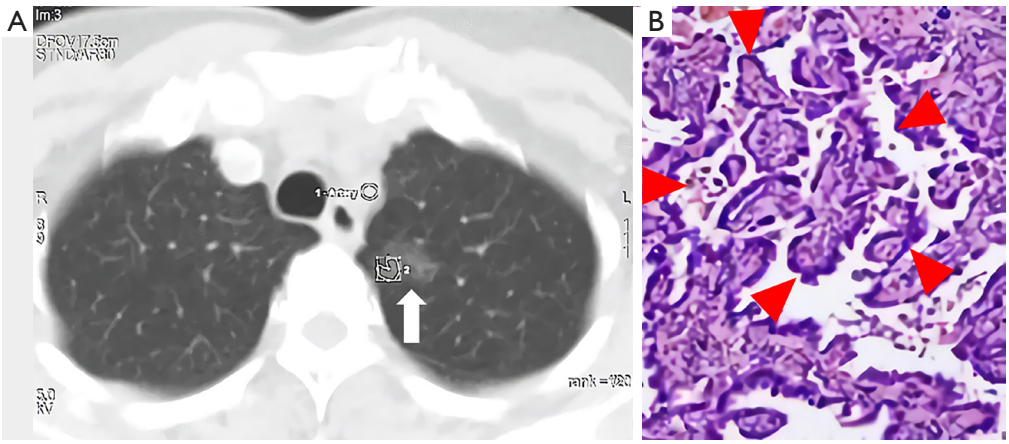

Figure 3 A 52-year-old female with MIA in the left upper lung was examined by spectral CT perfusion imaging. (A) The CT image of the patient. (B) The pathology image of the patient. (A) Axial CT image at the lung window revealed a pure ground-glass opacity in the left upper lobe (arrow). (B) The pathological specimen revealed MIA (red arrowheads) (H&E staining at ×400 magnification). The IRF TO value of this lesion was 2.61 s, which was correlated with the pathological diagnosis of low-invasive or non-invasive lesion. MIA, micro invasive lung adenocarcinoma; CT, computed tomography; H&E, hematoxylin and eosin; IRF TO, impulse residue function time of arrival.

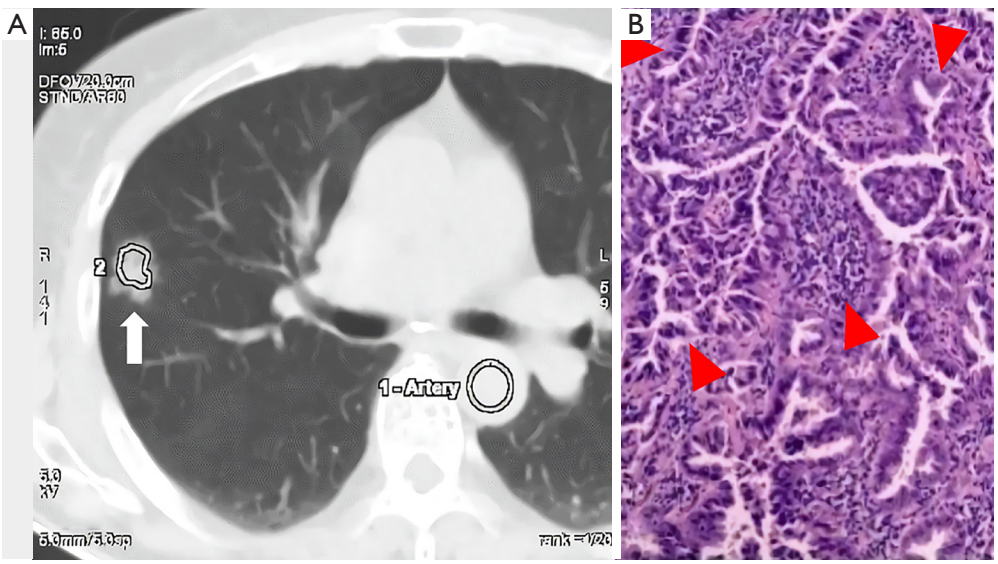

Figure 4 A 65-year-old female with IAC in the right upper lung was examined by spectral CT perfusion imaging. (A) The CT image of the patient. (B) The pathology image of the patient. (A) Axial CT at the lung window demonstrate a sub-solid nodule in the right upper lung (arrow). (B) IAC was confirmed by pathology (red arrowheads) (H&E staining at ×400 magnification). CT perfusion parameter IRF TO was 6.24 s. The IRF TO value was long, which indicated the diagnosis of invasive lesion. IAC, invasive lung adenocarcinoma; CT, computed tomography; H&E, hematoxylin and eosin; IRF TO, impulse residue function time of arrival.

density ratio, edge burr, lobulation, bronchial gas phase, and pleural traction, among others, can be used to estimate the invasiveness of LUAD (7,16-18). A previous study used texture analysis of high-resolution CT images to distinguish AIS, MIA, and IAC (19). It was possible to differentiate AIS-MIA from IAC using the 90th percentile CT numbers and entropy. Currently, although a few trials have studied the pathological invasion of LUAD using spectral CT imaging, there are no studies that have investigated CT perfusion imaging in the evaluation of pathological invasiveness of LUAD (20,21). It was postulated that the net enhancement value of CT or iodine-based map at a single energy level can be used to evaluate the invasiveness of LUAD (20,21). The net enhancement value of CT or iodine-based image is directly related to the distribution of intravascular and extracellular space in the tumor, which reflect the changes of tumor hemodynamics. Due to the vasculature differences between benign and malignant tumors, the CT parameters related to enhancement of these tumors also reflect the tumor invasiveness. Therefore, enhanced CT value was used to differentiate pulmonary nodules traditionally (22).

Studies of CT perfusion imaging showed that the spectral CT perfusion imaging was superior to that of the traditional CT enhancement value in evaluating the blood perfusion status and the invasiveness of pulmonary nodules. The sensitivity, specificity, and accuracy were 79–91%, 81–96%, and 80–96% respectively, for the differentiation of malignant from benign nodules (9,10). In this study, we discovered that IRF TO value of CT perfusion imaging was significantly different in AIS, MIA, and IAC (P=0.004). Histopathological study of LUAD also found that the microvessel density of different pathological subtypes of LUAD was different, and the microvessel density of solid LUAD was higher than that of non-solid LUAD (23). With the aggravation of the invasion of LUAD, the solid components gradually increased from AIS or MIA to IAC, which may be accompanied by the increase of microvessel density in the tumor. Our results show that there were no significant differences in BF, BV, MSI, MTT, PS, PEI, TTP, and Tmax among AIS, MIA, and IAC. The CT perfusion parameter IRF TO reflects the different changes of invasiveness exactly. The results of this study revealed that IRF TO increases with the increment of the invasiveness of LUAD. This may be attributed to the distinctive vascular distribution among different subtypes of LUAD, and quantitative study of microvessel density is warranted to investigate this issue.

For AIS, MIA, and IAC, IRF TO may indirectly reflect the potential tumor angiogenesis and vasculature distribution, and further indicates the differences of invasiveness of LUAD. In addition, the results of our study suggest that IRF TO contributes to differentiating precursor glandular lesions (AAH and AIS) from invasive LUAD (MIA and AIS) (*Tables 2-4*), the difference between which was statistically significant. Furthermore, a study had shown that the prognosis of solid LUAD was poor (24). Furthermore, MIA was separated from IAC and according to different prognosis, and combined AAH, and AIS as one group. The IRF TO of this group was significantly lower than that of IAC (P<0.001). These results may indicate that the quantitative parameter IRF TO of spectral CT perfusion imaging may be used to evaluate the prognosis of LUAD, which should be investigated in future studies.

There were some limitations in this study. The sample size, especially the number of AIS cases was too small, which could be attributed to the disease detection rate and the medical treatment rate. The correlation between the parameters of spectral CT perfusion imaging and the ratio of ground-glass component of LUAD was not analyzed in this study. The growth pattern of LUAD, such as adherent type, acinar type, papillary type, or solid growth, may also affect the outcomes, which was not examined in this study. Therefore, further studies should incorporate a larger sample size and more comprehensive pathological subtypes.

Conclusions

Spectral CT perfusion imaging has a potential application in the evaluation of the invasiveness of LUAD. The IRF TO value of spectral CT perfusion imaging increased with the increment of pathological invasiveness of adenocarcinoma, which may help to distinguish between AIS, MIA, and IAC.

Acknowledgments

Funding: This work was supported by 2019 SKY Imaging Research Fund of the Chinese International Medical Foundation (No. Z-2014-07-1912), Beijing Natural Science Foundation (No. Z200015), Beijing Municipal Administration of Hospitals Clinical Medicine Development of Special Funding Support (No. ZYLX201803), Beijing Hospitals Authority's Ascent Plan (No. DFL20191103), and the third round of Public Welfare Development And Reform Pilot Projects of Beijing Municipal Medical Research Institutes (Beijing Medical Research Institute, 2019-1).

Footnote

Reporting Checklist: The authors have completed the STROBE reporting checklist. Available at https://qims.amegroups.com/article/view/10.21037/qims-23-487/rc

Conflicts of Interest: All authors have completed the ICMJE uniform disclosure form (available at https://qims.amegroups.com/article/view/10.21037/qims-23-487/coif). The authors have no conflicts of interest to declare.

Ethical Statement: The authors are accountable for all aspects of the work in ensuring that questions related to the accuracy or integrity of any part of the work are appropriately investigated and resolved. The study was conducted in accordance with the Declaration of Helsinki (as revised in 2013). The study was approved by the Medical Ethics Committee of Peking University Cancer Hospital & Institute (No. 2021KT04), and written informed consent was provided by all patients.

References

1. Torre LA, Bray F, Siegel RL, Ferlay J, Lortet-Tieulent J, Jemal A. Global cancer statistics, 2012. CA Cancer J Clin 2015;65:87-108.
2. Chen W, Zheng R, Baade PD, Zhang S, Zeng H, Bray F, Jemal A, Yu XQ, He J. Cancer statistics in China, 2015. CA Cancer J Clin 2016;66:115-32.
3. Wang Y, Hou K, Jin Y, Bao B, Tang S, Qi J, Yang Y, Che X, Liu Y, Hu X, Zheng C. Lung adenocarcinoma-specific three-integrin signature contributes to poor outcomes by metastasis and immune escape pathways. J Transl Int Med 2021;9:249-63.
4. Travis WD, Brambilla E, Noguchi M, Nicholson AG, Geisinger KR, Yatabe Y, et al. International Association for the Study of Lung Cancer/American Thoracic Society/European Respiratory Society international multidisciplinary classification of lung adenocarcinoma. J Thorac Oncol 2011;6:244-85.
5. Nicholson AG, Tsao MS, Beasley MB, Borczuk AC, Brambilla E, Cooper WA, Dacic S, Jain D, Kerr KM, Lantuejoul S, Noguchi M, Papotti M, Rekhtman N, Scagliotti G, van Schil P, Sholl L, Yatabe Y, Yoshida A, Travis WD. The 2021 WHO Classification of Lung Tumors: Impact of Advances Since 2015. J Thorac Oncol 2022;17:362-87.
6. Van Schil PE, Asamura H, Rusch VW, Mitsudomi T, Tsuboi M, Brambilla E, Travis WD. Surgical implications of the new IASLC/ATS/ERS adenocarcinoma classification. Eur Respir J 2012;39:478-86.
7. Behera M, Owonikoko TK, Gal AA, Steuer CE, Kim S, Pillai RN, Khuri FR, Ramalingam SS, Sica GL. Lung Adenocarcinoma Staging Using the 2011 IASLC/ATS/ERS Classification: A Pooled Analysis of Adenocarcinoma In Situ and Minimally Invasive Adenocarcinoma. Clin Lung Cancer 2016;17:e57-64.
8. Takahashi M, Shigematsu Y, Ohta M, Tokumasu H, Matsukura T, Hirai T. Tumor invasiveness as defined by the newly proposed IASLC/ATS/ERS classification has prognostic significance for pathologic stage IA lung adenocarcinoma and can be predicted by radiologic parameters. J Thorac Cardiovasc Surg 2014;147:54-9.
9. Mirsadraee S, van Beek EJ. Functional imaging: computed tomography and MRI. Clin Chest Med 2015;36:349-63, x.
10. Chen ML, Sun YS. CT perfusion imaging: a valuable and feasible resolution of pulmonary nodules. Advanced Ultrasound in Diagnosis and Therapy 2019(02):27-34.
11. Chen ML, Wei YY, Li XT, Qi LP, Sun YS. Low-dose spectral CT perfusion imaging of lung cancer quantitative analysis in different pathological subtypes. Transl Cancer Res 2021;10:2841-8.
12. Ohno Y, Koyama H, Fujisawa Y, Yoshikawa T, Seki S, Sugihara N, Sugimura K. Dynamic contrast-enhanced perfusion area detector CT for non-small cell lung cancer patients: Influence of mathematical models on early prediction capabilities for treatment response and recurrence after chemoradiotherapy. Eur J Radiol 2016;85:176-86.
13. Ohno Y, Koyama H, Matsumoto K, Onishi Y, Takenaka D, Fujisawa Y, Yoshikawa T, Konishi M, Maniwa Y, Nishimura Y, Ito T, Sugimura K. Differentiation of malignant and benign pulmonary nodules with quantitative first-pass 320-detector row perfusion CT versus FDG PET/CT. Radiology 2011;258:599-609.
14. Bohlsen D, Talakic E, Fritz GA, Quehenberger F, Tillich

M, Schoellnast H. First pass dual input volume CT-perfusion of lung lesions: The influence of the CT- value range settings on the perfusion values of benign and malignant entities. Eur J Radiol 2016;85:1109-14.
15. Jiang C, Luo Y, Yuan J, You S, Chen Z, Wu M, Wang G, Gong J. CT-based radiomics and machine learning to predict spread through air space in lung adenocarcinoma. Eur Radiol 2020;30:4050-7.
16. Zhang Y, Shen Y, Qiang JW, Ye JD, Zhang J, Zhao RY. HRCT features distinguishing pre-invasive from invasive pulmonary adenocarcinomas appearing as ground-glass nodules. Eur Radiol 2016;26:2921-8.
17. Yanagawa M, Johkoh T, Noguchi M, Morii E, Shintani Y, Okumura M, Hata A, Fujiwara M, Honda O, Tomiyama N. Radiological prediction of tumor invasiveness of lung adenocarcinoma on thin-section CT. Medicine (Baltimore) 2017;96:e6331.
18. Son JY, Lee HY, Lee KS, Kim JH, Han J, Jeong JY, Kwon OJ, Shim YM. Quantitative CT analysis of pulmonary ground-glass opacity nodules for the distinction of invasive adenocarcinoma from pre-invasive or minimally invasive adenocarcinoma. PLoS One 2014;9:e104066.
19. Yagi T, Yamazaki M, Ohashi R, Ogawa R, Ishikawa H, Yoshimura N, Tsuchida M, Ajioka Y, Aoyama H. HRCT texture analysis for pure or part-solid ground-glass nodules: distinguishability of adenocarcinoma in situ or minimally invasive adenocarcinoma from invasive adenocarcinoma. Jpn J Radiol 2018;36:113-21.
20. Zhang Y, Tang J, Xu J, Cheng J, Wu H. Analysis of pulmonary pure ground-glass nodule in enhanced dual energy CT imaging for predicting invasive adenocarcinoma: comparing with conventional thin-section CT imaging. J Thorac Dis 2017;9:4967-78.
21. Son JY, Lee HY, Kim JH, Han J, Jeong JY, Lee KS, Kwon OJ, Shim YM. Quantitative CT analysis of pulmonary ground-glass opacity nodules for distinguishing invasive adenocarcinoma from non-invasive or minimally invasive adenocarcinoma: the added value of using iodine mapping. Eur Radiol 2016;26:43-54.
22. Ohno Y, Nishio M, Koyama H, Miura S, Yoshikawa T, Matsumoto S, Sugimura K. Dynamic contrast-enhanced CT and MRI for pulmonary nodule assessment. AJR Am J Roentgenol 2014;202:515-29.
23. Maeda R, Ishii G, Ito M, Hishida T, Yoshida J, Nishimura M, Haga H, Nagai K, Ochiai A. Number of circulating endothelial progenitor cells and intratumoral microvessel density in non-small cell lung cancer patients: differences in angiogenic status between adenocarcinoma histologic subtypes. J Thorac Oncol 2012;7:503-11.
24. Barletta JA, Yeap BY, Chirieac LR. Prognostic significance of grading in lung adenocarcinoma. Cancer 2010;116:659-69.

Cite this article as: Chen ML, Liu YL, Zhu HB, Li XT, Qi LP, Sun YS. The differential diagnosis of lung precursor glandular lesions, micro-invasive adenocarcinoma, and invasive adenocarcinoma using low dose spectral computed tomography perfusion imaging. Quant Imaging Med Surg 2024;14(1):814-823. doi: 10.21037/qims-23-487

